Disordered ground state in a spin-orbit coupled pseudospin-$\frac{1}{2}$ cobalt-based metal-organic framework magnet with orthogonal spin dimers

Sebin J. Sebastian,[1] S. Mohanty,[1] A. Nath,[2] M. P. Saravanan,[3] S. Mandal,[2] A. A. Tsirlin,[4] and R. Nath[1,*]

[1]*School of Physics, Indian Institute of Science Education and Research, Thiruvananthapuram 695551, India*
[2]*School of Chemistry, Indian Institute of Science Education and Research, Thiruvananthapuram 695551, India*
[3]*UGC-DAE Consortium for Scientific Research, University Campus, Khandwa Road, Indore 452001, India*
[4]*Felix Bloch Institute for Solid-State Physics, Leipzig University, 04103 Leipzig, Germany*

(Received 28 November 2023; revised 22 January 2024; accepted 20 February 2024; published 15 March 2024)

We present the magnetic properties of a quantum dimer magnet based on Co^{2+}. The metal-organic framework compound $Co_2(BDC)_2(DPTTZ)_2 \cdot DMF$ features Co^{2+} dimers arranged nearly orthogonal to each other, similar to the Shastry-Sutherland lattice. Our assessment based on the magnetization and heat capacity experiments reveals that the magnetic properties at low temperatures can be described by pseudospin-1/2. The magnetic ground state of the material is found to be a singlet with a tiny spin gap. The thermodynamic properties are described by a model of isolated spin dimers with the anisotropic exchange couplings $J_{xy} \simeq 3.5$ K and $J_z \simeq 11$ K. Interestingly, no field-induced quantum phase transition is detected down to 100 mK around the critical field of gap closing, suggesting the absence of Bose-Einstein condensation of triplons and establishing isolated dimers with a negligible interdimer coupling.

DOI: 10.1103/PhysRevMaterials.8.034403

I. INTRODUCTION

A quantum phase transition (QPT) is a transition between two phases at absolute zero temperature driven by quantum fluctuations [1]. Such a phase can be accessed upon variation of an external control parameter that has direct bearing on the system properties. Antiferromagnetic (AFM) spin-1/2 dimers are well suited to study QPT because they are characterized by a singlet ($|S, S_z\rangle = |0, 0\rangle$) ground state with entangled spins and an excitation gap in the energy spectrum [2]. Application of an external magnetic field leads to a closing of the excitation gap and stabilizes the magnetic long-range order (LRO). In a Heisenberg magnet, this nontrivial field-induced LRO can be described well as the Bose-Einstein condensation (BEC) of spin-1 triplons [2–4]. Experimentally, BEC physics is demonstrated in compounds featuring coupled spin dimers, even-leg ladders, and bond-alternating spin chains [5–10]. Another fascinating field-induced quantum effect is the appearance of magnetization plateaus, typically observed in spin systems with orthogonal dimers, such as the Shastry-Sutherland lattice $SrCu_2(BO_3)_2$ [11,12].

In the past, oxide materials with several transition-metal and few rare-earth ions (e.g., Yb^{3+}) have been studied in the context of field-induced transitions [8,13–18]. Among these systems, Co^{2+}-based compounds are quite attractive as they show pseudospin-$\frac{1}{2}$ behavior at low temperatures, similar to Yb^{3+} ($4f$) and Ce^{3+} ($4f$) magnets [18–20], single-ion anisotropy [21], etc. Spin-orbit coupling (SOC) combined with peculiarities of the crystal electric field (CEF) gives rise to bond-dependent anisotropy of the exchange couplings, thus offering a promising playground to realize exotic phases, including the field-induced quantum spin liquid (QSL) in Kitaev materials [22,23], BEC of triplons [24], and Berezinskii-Kosterlitz-Thoueless (BKT) transition [25]. Recently, BEC of triplons has been observed in a $4f$-based dimer magnet $Yb_2Si_2O_7$, but with an unusually asymmetric BEC dome [18]. This asymmetry is sometimes attributed to the anisotropy in the exchange parameters of the Hamiltonian [26,27]. Similar physics is also envisaged for Co^{2+}-based compounds because of the exchange anisotropy [28]. In this regard, Co^{2+}-based metal-organic compounds are ideal contenders and provide a convenient testing ground for field-induced studies, owing to the reduced exchange couplings compared to their inorganic counterparts. This leads to lower critical fields, thus facilitating experimental access to the complete phase diagram using continuous-field laboratory magnets [15,16,29].

In this paper, we report the structural and magnetic properties of a Co^{2+}-based metal-organic framework $Co_2(BDC)_2(DPTTZ)_2 \cdot DMF$ (abbreviated as Co-MOF), investigated via magnetization and heat capacity measurements down to 100 mK, followed by exact diagonalization calculations. Co-MOF crystallizes in an orthorhombic space group *Iba*2 (No. 45) with the lattice parameters $a = 34.7269(1)$ Å, $b = 17.1760(3)$ Å, $c = 17.0489(5)$ Å, and $\alpha = \beta = \gamma = 90^\circ$ [30,31]. It contains two crystallographically nonequivalent cobalt atoms, Co(1) and Co(2). Each Co(II) center is coordinated with O and N atoms in a distorted heteroleptic octahedron (CoO_4N_2) geometry with Co–O and Co–N distances in the ranges of 1.988(4)–2.232(4) Å and 2.134(3)–2.160(3) Å, respectively. Two nonequivalent cobalt octahedra are connected via two C atoms and form a Co(1)–Co(2) dimer. These dimer units are further connected through a phenyl ring of benzene dicarboxylate (BDC) ligands to form a corrugated

*rnath@iisertvm.ac.in

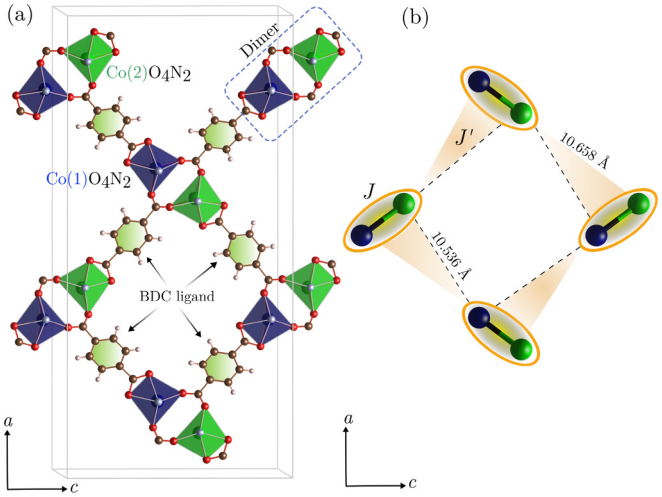

FIG. 1. (a) Structure of Co-MOF in one unit cell showing the formation of spin dimers by the CoO_4N_2 units and the interdimer connectivity. (b) Schematic diagram showing the orthogonal arrangement of dimers and the possible exchange couplings.

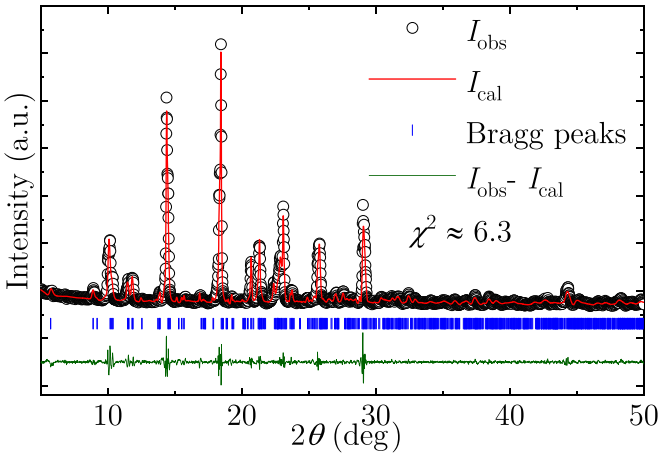

FIG. 2. Powder XRD pattern of Co-MOF measured at room temperature. The open circles represent the experimental data and the solid red line represents the Le Bail fit. The Bragg positions are indicated by blue vertical bars and the bottom solid green line indicates the difference between the experimental and calculated intensities.

two-dimensional layer [Fig. 1(a)]. Each layer is pillared by DPTTZ (*N*, *N*′-di(4-pyridyl)thiazolo-[5,4-d] thiazole) units to form an overall three-dimensional framework. Interestingly, these Co–Co dimers are arranged in an orthogonal fashion, reminiscent of the famous Shastry-Sutherland lattice [see Fig. 1(b)]. However, due to reduced crystal symmetry, the dimers are slightly deviating from perfect orthogonality. The possible intradimer interaction J ($d_{\mathrm{Co-Co}} \simeq 4.04$ Å) and interdimer interaction J' ($d^{\mathrm{avg}}_{\mathrm{Co-Co}} \simeq 10.597$ Å) are also depicted in Fig. 1(b).

II. METHODS

The single-crystal synthesis of Co-MOF involves two steps. In the first step, the precursor DPTTZ was prepared by mixing 200 mg of dithiooxamide and 0.4 mL of 4-pyridinecarboxaldehyde in 10 mL of high-performance liquid chromatography *N*, *N*′-dimethylformamide (DMF), and refluxed at 153 °C for 5 h [32]. The yellow-colored needle-shaped crystals of DPTTZ were formed after slow cooling. The crystals were washed in water, dried under vacuum, and stored under ambient conditions. In the second step, 0.027 mmol (7.85 mg) $Co(NO_3)_2.6H_2O$, 0.03 mmol (4.98 mg) terephthalic acid, and 0.025 mmol (7.4 mg) DPTTZ were mixed in 2:0.5 DMF : H_2O ratio and sonicated for 1 h. The resulting solution was transferred to a Teflon-lined vessel and kept in an autoclave at 100 °C for two days. Co-MOF crystals were obtained after slow cooling of the autoclave. The crystals were washed several times with DMF and dried under vacuum. The crystals were maintained under ambient conditions prior to further experiments. A large number of small single crystals were crushed into fine powder and the phase purity of the product was confirmed via powder x-ray diffraction (XRD) at room temperature using a PANalytical x-ray diffractometer (CuK_α radiation, $\lambda_{\mathrm{avg}} \simeq 1.5418$ Å). Le Bail analysis of the powder XRD pattern was performed using the MAG2POL software package [33]. Figure 2 shows the powder XRD data collected at $T = 300$ K along with the fit. The structural parameters given in Ref. [30] were used as the initial parameters. The obtained lattice parameters $a = 34.9769(1)$ Å, $b = 17.1990(1)$ Å, $c = 17.1076(1)$ Å, and $\alpha = \beta = \gamma = 90°$ are in close agreement with the previous report [30].

DC magnetization (M) of the powder sample was measured using a superconducting quantum interference device (SQUID) magnetometer (MPMS-3, Quantum Design). The measurements were performed in the temperature range of $1.8 \leqslant T \leqslant 380$ K and in the magnetic field range of $0 \leqslant H \leqslant 7$ T. The SQUID enabled us to measure the isothermal magnetization at $T = 0.4$ K with the help of a ^{3}He attachment. Heat capacity (C_p) was measured on a small piece of sintered pellet using the thermal relaxation technique over a large temperature range in two physical property measurement systems (PPMS, Quantum Design). For $T > 2$ K, measurements were done in a 9 T PPMS, while for $0.1 \leqslant T \leqslant 4$ K, we have used a dilution insert in a 14 T PPMS.

The magnetization and heat capacity of the anisotropic spin dimer are simulated via exact diagonalization using the `fulldiag` utility of the ALPS package [34], where the number of sites is taken to be $Z = 2$.

III. RESULTS

A. Magnetization

Temperature-dependent magnetic susceptibility χ ($\equiv M/H$) measured in different magnetic fields is shown in Fig. 3(a). At the lowest measured field ($\mu_0 H = 0.01$ T), $\chi(T)$ passes through a broad maximum at $T_\chi^{\mathrm{max}} \simeq 3$ K, which is the signature of an antiferromagnetic (AFM) short-range order, typical for a low-dimensional spin system. With increasing field, the position of the broad maximum shifts toward low temperature, as expected. Below 3 K, $\chi(T)$ exhibits a rapid decrease, suggesting a singlet ground state or the opening of a spin gap, which necessitates additional investigation [35,36]. No anomaly associated with the magnetic LRO is observed down to 1.8 K.

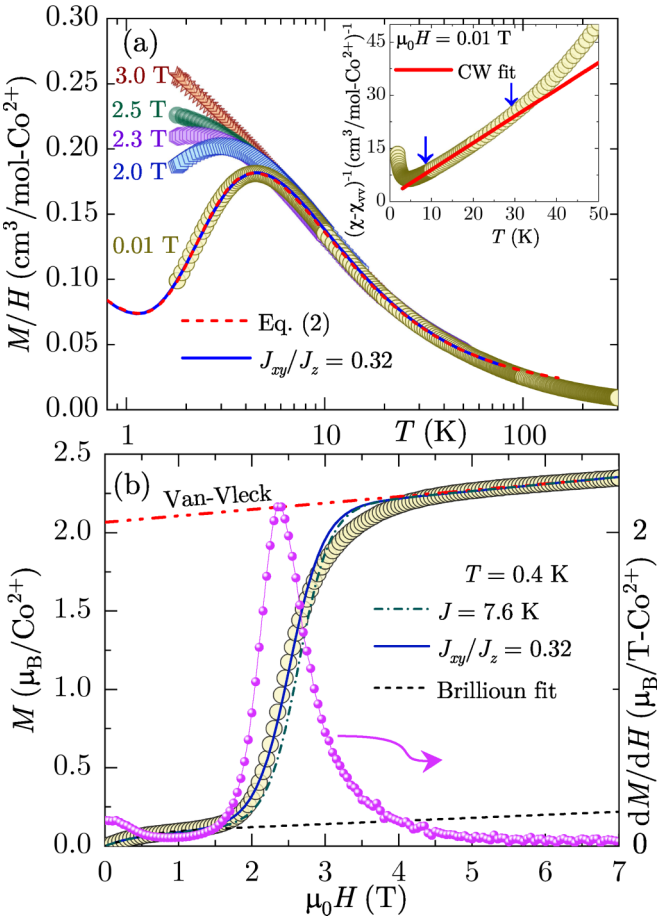

FIG. 3. (a) $\chi(T)$ of Co-MOF measured in different applied fields. The dash-dotted line represents the fit of the $\mu_0 H = 0.01$ T data by the interacting dimer model [Eq. (2)], while the solid line is the simulation of isolated spin dimers with anisotropic interactions ($J_z = 11$ K and $J_{xy} = 3.52$ K). Inset: CW fit to the low-T $1/\chi$ data (after subtracting the van Vleck contribution). (b) M vs H and dM/dH vs H on the left and right y axes, respectively, measured at $T = 0.4$ K. The horizontal dash-dotted line marks the van Vleck contribution. The dashed line shows the Brillouin fit [Eq. (4)] to magnetization in the gapped regime. The dash-dotted and solid lines are the simulations for isolated spin dimers with isotropic and anisotropic interactions, respectively.

To extract key magnetic parameters, we analyzed $\chi(T)$ using the modified Curie-Weiss (CW) law

$$\chi(T) = \chi_0 + \frac{C}{T - \theta_{\rm CW}}, \tag{1}$$

where χ_0 is the temperature-independent contribution consisting of the core diamagnetic susceptibility ($\chi_{\rm core}$) and van Vleck paramagnetism ($\chi_{\rm VV}$) of the open shell of the Co^{2+} ions present in the sample. The second term in Eq. (1) represents the CW law with the Curie constant $C = N_{\rm A}\mu_{\rm eff}^2/3k_{\rm B}$, where $N_{\rm A}$ is the Avogadro's number, $k_{\rm B}$ is the Boltzmann constant, $\mu_{\rm eff} = g\sqrt{S(S+1)}\mu_{\rm B}$ is the effective magnetic moment, g is the Landé g-factor, $\mu_{\rm B}$ is the Bohr magneton, S is the spin quantum number, and $\theta_{\rm CW}$ is the characteristic CW temperature. Above 150 K, $\chi(T)$ for $\mu_0 H = 0.01$ T was fitted by Eq. (1) that yields $\chi_0 \simeq 7.3 \times 10^{-4}$ cm^3/mol, the high-T (HT) effective moment $\mu_{\rm eff}^{\rm HT} \simeq 4.53$ $\mu_{\rm B}$/Co^{2+}, and the high-T CW temperature $\theta_{\rm CW}^{\rm HT} \simeq -4$ K. The value of $\mu_{\rm eff}^{\rm HT}$ corresponds to $J_{\rm eff} = 3/2$ with $g \simeq 2.33$ for the $3d^7$ configuration. A slightly larger $\mu_{\rm eff}^{\rm HT}$ value compared with the theoretical spin-only value ($\sim$3.87 μ_B/Co^{2+} for $J_{\rm eff} = 3/2$ with $g = 2.0$) indicates anisotropy in the g-factor stemming from the pseudotrigonal crystal field as well as additional orbital contribution, as observed in several Co^{2+}-based systems [37,38].

At temperatures below 40 K, $1/\chi$ exhibits a subtle slope change, deviating from the high-T CW behavior. Spin-orbit coupling splits the Co^{2+} multiplet into several Kramers doublets, and the physics at low temperatures is fully determined by the lowest Kramers doublet that can be treated as pseudospin-$\frac{1}{2}$. This type of crossover from the high-T $S = 3/2$ to the low-T pseudospin-1/2 behavior is a common character of Co^{2+}-based compounds [39–41]. To understand the low-temperature $\chi(T)$ data precisely, one requires a proper estimation of $\chi_{\rm VV}$ that arises from excitations between the lowest Kramers doublet and excited states. After subtracting $\chi_{\rm VV}$ (obtained from the magnetization isotherm at $T = 0.4$ K) from $\chi(T)$, $1/(\chi - \chi_{\rm VV})$ shows a clear slope change and a linear regime below 40 K [inset of Fig. 3(a)]. A CW fit [Eq. (1)] in the low-T (LT) regime (8–30 K) returns $\mu_{\rm eff}^{\rm LT} \simeq 3.40$ $\mu_{\rm B}$/Co^{2+} and $\theta_{\rm CW}^{\rm LT} \simeq -1.9$ K. The $\mu_{\rm eff}^{\rm LT}$ value corresponds to a pseudospin-1/2 with an average $g \simeq 3.93$. Such a large value of g compared to the free-electron value $g = 2$ reflects the effect of spin-orbit coupling [40–43]. The negative value of $\theta_{\rm CW}^{\rm LT}$ confirms the dominant AFM interactions at low temperatures.

From the crystal structure, while considering the spin lattice of Co atoms, we anticipate the formation of magnetic dimers of Co^{2+} ions in an orthogonal fashion, reminiscent of the Shastry-Sutherland lattice. As a first step, to determine the potential exchange couplings, we fitted the $\chi(T)$ data using the following expression:

$$\chi(T) = \chi_0 + \frac{C_{\rm imp}}{T - \theta_{\rm imp}} + \chi_{\rm d}(T). \tag{2}$$

Here, the second term is the CW law that takes into account the impurity contributions and $\chi_{\rm d}(T)$ is the expression for the susceptibility of an AFM spin-1/2 coupled dimer model, which has the form [44]

$$\chi_{\rm d}(T) = \frac{N_{\rm A} g^2 \mu_{\rm B}^2}{k_{\rm B}T[3 + \exp(J/k_{\rm B}T) + zJ'/k_{\rm B}T]}. \tag{3}$$

Here, $J/k_{\rm B}$ is the intradimer exchange coupling, $J'/k_{\rm B}$ represents the interdimer exchange coupling, and z is the number of nearest-neighbor spins. The fit using Eq. (2) in the low-temperature regime ($1.80 \leqslant T \leqslant 40$ K) [see Fig. 3(a)] returns $\chi_0 \simeq 0.0133$ cm^3/mol, $C_{\rm imp} \simeq 0.077$ cm^3-K/mol, the effective interaction strength between impurity spins $\theta_{\rm imp} \simeq -0.3$ K, $g \simeq 4.15$, $z = 2$, $J/k_{\rm B} \simeq 7.6$ K, and $J'/k_{\rm B} \simeq 0.07$ K. The obtained value of $C_{\rm imp}$ corresponds to $\sim$4.5% of spin-1/2 impurities. The value of $J/k_{\rm B} \simeq 7.6$ K with $g \simeq 4.15$ sets the critical field of gap closing $H_{\rm C1} = \Delta_0/g\mu_{\rm B} \simeq 2.7$ T, where $\Delta_0 \simeq J/k_B$ is the spin gap between the singlet and triplet states of the dimer [9].

To track the magnetization response with respect to the applied field, we measured an isothermal magnetization [$M(H)$] at $T = 0.4$ K up to 7 T. For a gapped spin system, magnetization (M) typically remains zero below H_{C1}, while above this field, it is expected to increase up to the saturation field H_{C2} that marks the onset of the fully polarized state [45,46]. As shown in Fig. 3(b), in the low-field regime, M exhibits a wide plateau up to $H \sim 2$ T, clearly suggesting a singlet ground state, and the critical field required to overcome the spin gap is about $H_{C1} \simeq 2$ T. This plateau with nonzero magnetization can be attributed to the paramagnetic impurities/defects expected in a powder sample, which saturate above 1 T. Above $H_{C1} \simeq 2$ T, M increases sharply and saturates in high fields. It is also observed that M increases weakly with increasing field beyond the saturation field H_{C2}. This weak increase in high fields is primarily due to the van Vleck contribution (χ_{VV}), expected for Co^{2+} systems in an octahedral environment [47]. The slope and y intercept of a linear fit to the data above ~4 T yields $\chi_{VV} \simeq 2.46 \times 10^{-2}$ cm^3/mol and the saturation magnetization of $M_S \simeq 2.05$ μ_B/f.u., respectively. This value of M_S is in good agreement with $M_{sat} = gJ_{eff}\mu_B \simeq 2.0$ μ_B expected for a pseudospin-1/2 with the powder-averaged $g \simeq 4.0$. Thus, the magnetization isotherm analysis also validates the pseudospin-1/2 picture of the Co^{2+} magnetism at low temperatures.

In order to quantitatively estimate the impurity contribution and to visualize zero magnetization below H_{C1}, we fitted the data below 2 T [see Fig. 3(b)] by the following equation [9]:

$$M = \chi H + N_A \mu_B f_{imp} S_{imp} g_{imp} \times B(x), \tag{4}$$

where χ is the intrinsic susceptibility of the sample, f_{imp} is the molar fraction of the impurities, g_{imp} is the impurity g-factor, S_{imp} represents the impurity spin, $B(x)$ is the Brillouin function taken for the spin value $S_{imp}(x)$, and the argument (x) can be defined by $x = g_{imp}\mu_B S_{imp} H/[k_B(T - \theta_{imp})]$. The fit yields the following parameters: $f_{imp} = 0.039(4)$, $S_{imp} = 0.5$, $g_{imp} = 4.15(8)$, and $\theta_{imp} = -0.45(8)$ K. This amount of impurity matches the one found from the susceptibility fit. Further, after subtracting the impurity contribution, the corrected magnetization stays at zero value up to H_{C1}, as expected in the gapped state.

B. Heat capacity

The temperature-dependent heat capacity [$C_p(T)$] measured in zero field and down to 100 mK is shown in Fig. 4(a). It depicts a well-defined broad maximum at around ~3 K, a hallmark of short-range AFM order. No signature of a magnetic LRO is observed down to the lowest temperature. At very low-Ts, a slight upturn is observed, which we attribute to the nuclear contribution appearing due to a small hyperfine field produced by Co or other atoms present. One can estimate the nuclear contribution by fitting the zero-field $C_p(T)$ data at very low temperatures with $C_n(T) = \alpha_Q/T^2$, where the coefficient α_Q is related to the nuclear-level splitting, both quadrupolar and Zeeman. In our zero-field data, the nuclear Schottky contribution dominates below 0.15 K. As our low-T data are available down to 0.1 K only, instead of fitting, we simulated the nuclear contribution by taking $\alpha_Q = 4 \times 10^{-4}$ J K/mol [inset of Fig. 4(a)], reported for

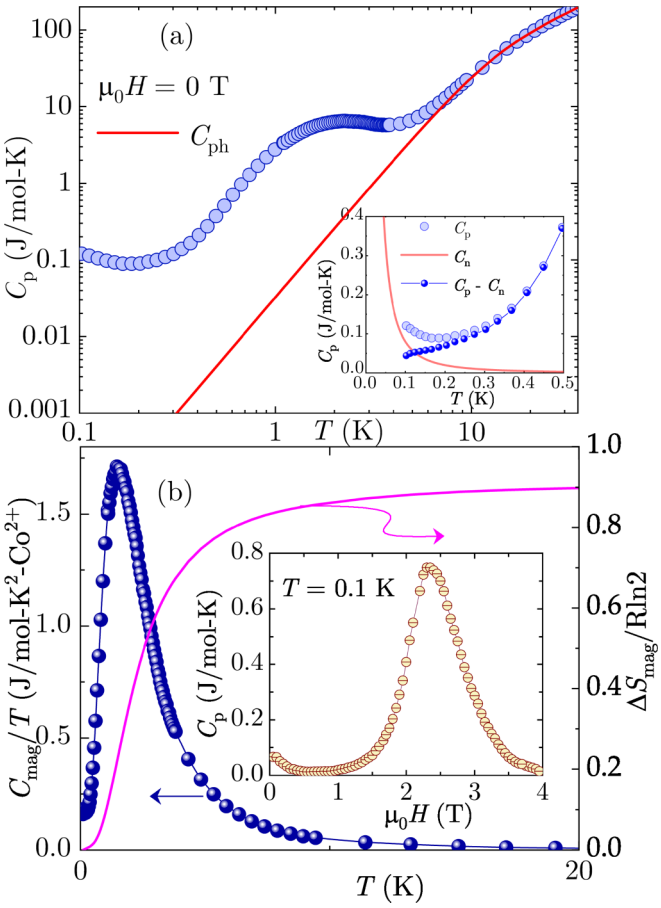

FIG. 4. (a) C_p vs T measured in zero-field along with the calculated phonon contribution C_{ph}. Inset: Zero-field $C_p(T)$ in the low-temperature regime with the solid line representing the nuclear contribution C_n. (b) C_{mag}/T and ΔS_{mag} vs T on the left and right y axes, respectively. Inset: $C_p(H)$ measured at $T = 0.1$ K.

$CeCoIn_5$ [48]. The data after subtraction of the nuclear contribution are also presented in the inset of Fig. 4(a), where C_p decreases towards zero on cooling, thus reflecting the singlet ground state.

In general, for a magnetic insulator, $C_p(T)$ in zero field has two major contributions, i.e., the phononic $C_{ph}(T)$ and magnetic $C_{mag}(T)$ parts. Above 10 K, $C_p(T)$ is dominated by C_{ph}, while at low temperatures, the dominant contribution is due to C_{mag}. To estimate $C_{ph}(T)$, experimental heat capacity data above 10 K were fitted empirically using a polynomial of the form [49]

$$C_{ph}(T) = aT^3 + bT^5 + cT^7 + dT^9. \tag{5}$$

From the fit [Fig. 4(a)], the obtained coefficients are $a = 3.3(1) \times 10^{-2}$ J mol^{-1} K^{-4}, $b = -1.1(1) \times 10^{-4}$ J mol^{-1} K^{-6}, $c = 2.1(4) \times 10^{-7}$ J mol^{-1} K^{-8}, and $d = -2.2(4) \times 10^{-10}$ J mol^{-1} K^{-10}. C_{mag} was obtained by subtracting C_{ph} and C_n from the total C_p. Furthermore, $C_{mag}(T)$ was used to estimate the magnetic entropy [$\Delta S_{mag}(T)$] by integrating $C_{mag}(T)/T$ in the measured T range. As shown in the right y axis in Fig. 4(b), $\Delta S_{mag}(T)$ $[= \int_{0.1\,K}^{T} \frac{C_{mag}(T')}{T'} dT']$ reaches a well-defined plateau close to 90% of $R \ln 2$, expected for spin-$\frac{1}{2}$. This again

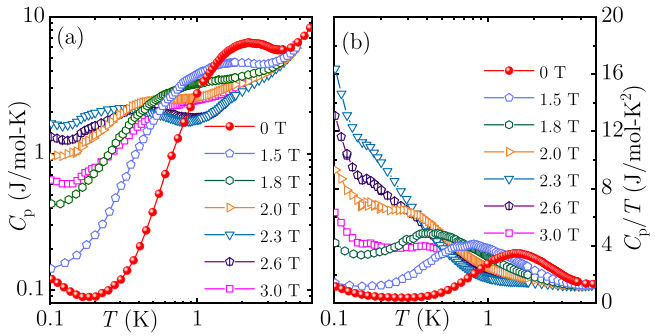

FIG. 5. (a) C_p vs T measured at low temperatures in different applied fields. (b) C_p/T vs T in the same temperature range.

indicates that the low-temperature properties of Co-MOF are governed by pseudospins-1/2 on the Co^{2+} ions [41]. In order to detect possible field-induced phases between H_{C1} and H_{C2}, we also measured $C_p(T)$ in different fields at low temperatures [see Fig. 5(a)]. With the application of field, the broad maximum shifts toward low temperatures, as expected for an AFM short-range order. No feature/peak of field-induced magnetic LRO reminiscent of BEC of triplons is observed down to 100 mK for $H > H_{C1}$. In order to visualize the absence of magnetic LRO, in Fig. 5(b), we plotted C_p/T vs T measured in various applied fields that display no clear anomaly. The absence of a field-induced magnetic LRO suggests almost noninteracting dimers.

C. Discussion

According to the Hund's rules, free Co^{2+} ions ($3d^7$) adopt the ^4F state with the orbital angular momentum $L = 3$ and total spin $S = 3/2$. This multiplet is split by the crystal field as well as SOC. In Fig. 6, we show the typical energy-level diagram of a Co^{2+} ion in the crystal-field environment. The cubic crystal field (CF) splits the ^4F multiplet into three multiplets: $^4A_{2g}$, $^4T_{2g}$, and $^4T_{1g}$. For the octahedral geometry, the $^4T_{1g}$ multiplet is expected to be stabilized. The energy level ($^4T_{1g}$) is further influenced by the SOC ($\hat{\mathcal{H}}_{SOC} = \lambda L \cdot S$), which

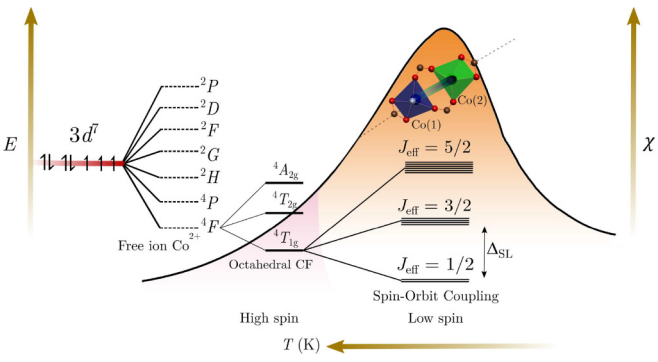

FIG. 6. The tentative energy diagram that depicts the splitting of the ^4F state of Co^{2+} under an octahedral crystal field and of the $^4T_{1g}$ state under SOC. $\chi(T)$ ($\mu_0 H = 0.01$ T) is plotted in the right y axis in order to visualize the temperature regimes where the whole multiplet and the lowest Kramers doublet (pseudospin-1/2) are effective, respectively. The maximum in $\chi(T)$ is arising due to the spin dimers.

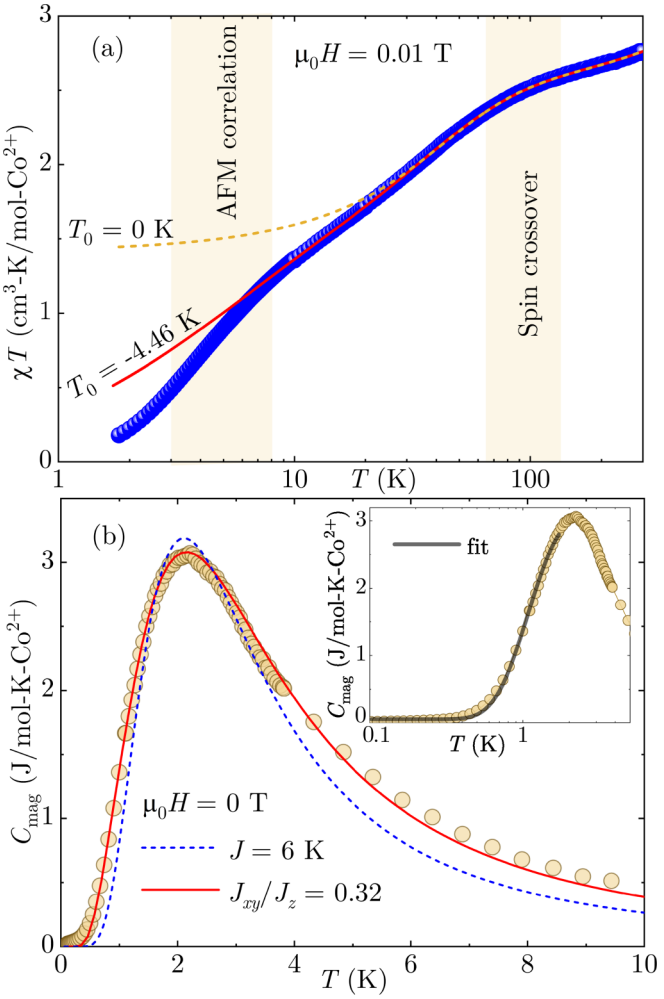

FIG. 7. (a) χT vs T is plotted for $\mu_0 H = 0.01$ T. The solid and dashed lines are fits using Eq. (6) for $T_0 = 0$ and $T_0 = -4.46$ K, respectively. (b) C_{mag} vs T measured down to 0.1 K in zero field. The dashed and solid lines represent the simulated curves for an isolated spin-1/2 dimer with isotropic ($J = 6$ K) and anisotropic ($J_z = 11$ K and $J_{xy} = 3.52$ K) interactions, respectively. Inset: Zero-field $C_{mag}(T)$ in the low-T regime; the solid line is an exponential fit with $\Delta_0^C/k_B \simeq 4.3$ K.

splits this level into a doublet, quartet, and sextet (six Kramers doublets in total). The lowest-lying doublet is separated from the quartet by an energy gap of $\Delta_{SL} = \frac{3}{2}\lambda$. Thus, when the temperature is much lower than the spin-orbit coupling λ (i.e., $T \ll |\lambda|/k_B$), one expects the magnetism to be determined by the lowest Kramers doublet [21,50]. Indeed, all our thermodynamic measurements confirm the pseudospin-1/2 nature of the local magnetic moment in Co-MOF. Upon revisiting the χT vs T data [Fig. 7(a)], we observed distinct slope changes that indicate changes in the effective magnetic moment of Co^{2+}. The temperature dependence can be fitted assuming excitations over the gap of Δ_{SL}/k_B as [51]

$$\chi = \chi_0 + \frac{N}{k_B(T - T_0)}\left[C_0 + C_1\left(\frac{2k_BT}{\Delta_{SL}}\right)\tanh\left(\frac{\Delta_{SL}}{2k_BT}\right) + C_2\tanh\left(\frac{\Delta_{SL}}{2k_BT}\right)\right]. \quad (6)$$

The value of N represents the number of paramagnetic entities, the coefficients C_0, C_1, and C_2 reflect the nature of the lowest-lying doublet and the first excited state, and T_0 essentially represents the energy scale of the exchange interactions. The fit above 10 K, as shown in Fig. 7(a), returns $\chi_0 \simeq 8.746 \times 10^{-4}$ cm^3/mol, $C_0/k_B \simeq 0.972$ cm^3 K/mol, $C_1/k_B \simeq 0.668$ cm^3 K/mol, $C_2/k_B \simeq 0.249$ cm^3 K/mol, and $\Delta_{SL}/k_B \simeq 160$ K with $T_0 \simeq -4.4$ K. The resulting value of Δ_{SL} confirms that at $T \ll \Delta_{SL}/k_B$, the system should behave as pseudospin-1/2. Indeed, our analysis below 30 K confirms this scenario. The negative value of T_0 suggests AFM correlations at low temperatures. In the low-T regime when $T \ll \Delta_{SL}/k_B$, the second term within the parentheses in Eq. (6) is almost negligible and provides an effective Curie constant of $C_{eff} = C_0/k_B + C_2/k_B \simeq 1.22$ cm^3 K/mol. This value corresponds to $\mu_{eff} \simeq 3.12\ \mu_B$ that matches closely with μ_{eff}^{LT} obtained from the CW fit.

Structurally, Co-MOF presents an ideal case of isolated dimers. Though the isolated dimer model with the isotropic (Heisenberg) intradimer interaction fits the $\chi(T)$ data reasonably well, it fails to reproduce the shape of the magnetization isotherm and $C_{mag}(T)$. A more narrow maximum is expected in the heat capacity of a Heisenberg spin dimer. Even if we choose $J = 6$ K instead of $J = 7.6$ K from the $\chi(T)$ fit in order to reproduce the position of the maximum, its height should be reduced by 25%, which is inconsistent with the almost full magnetic entropy recovered in our measurements. Despite all these adjustments, the peak remains more narrow than in the experiment, thus suggesting that Co-MOF cannot be treated as a Heisenberg spin dimer.

The heteroleptic, distorted CoO_4N_2 octahedron is elongated along the z direction as compared to the xy plane. This implies that a trigonal crystal-field splitting (CFS) is likely to develop. It leads to a Hamiltonian of the form $\hat{\mathcal{H}}_{trig} = \delta(3L_z^2 - 2)$, where δ denotes the strength of the CFS [52]. It is theoretically predicted that under the influence of trigonal distortion, isotropic Heisenberg exchange gives way to an anisotropic one described by the *XXZ* model [23]. Therefore, in Fig. 7(b), we simulated the $C_{mag}(T)$ using such a model

$$\hat{\mathcal{H}} = J_{xy}\left(S_i^x S_j^x + S_i^y S_j^y\right) + J_z S_i^z S_j^z, \tag{7}$$

with the exchange couplings $J_{xy} \simeq 3.5$ K and $J_z \simeq 11$ K. The anisotropy of $J_{xy}/J_z \simeq 0.32$ controls the width and height of the maximum, so it can be determined quite accurately even from powder data. With the *XXZ* model, we are also able to replicate $\chi(T)$ and M vs H curves using the same exchange parameters assuming isotropic $g = 4.15$ (see Fig. 3) and the same impurity as well as van Vleck contributions as in Sec. III A. The average exchange coupling $J_{avg}/k_B = \frac{2J_{xy}+J_z}{3k_B} \simeq 6$ K with $g = 4.15$ corresponds to $H_{C1} \simeq 2$ T. Similar physics of isolated spin dimers with anisotropic interactions is also realized in $4f$ systems, such as $BiYbGeO_5$ and $NaLu_{0.9}Yb_{0.1}Se_2$ [20,53].

We further quantified the spin gap by fitting $C_{mag}(T)$ by the low-T approximation of the isotropic spin-1/2 dimer model: $C_{mag} \propto (\Delta_0^C/k_BT)^2 e^{-\Delta_0^C/k_BT}$ [15]. The fit below 2 K [inset of Fig. 7(b)] returns $\Delta_0^C/k_B = 4.3(1)$ K, which is consistent with the spin gap of an anisotropic spin dimer, $\Delta_0/k_B = J_{xy} = 3.5$ K.

The scenario of isolated spin dimers is further confirmed from the magnetization isotherm and C_p vs H measurements. In the magnetization isotherm, the spacing between H_{C1} and H_{C2} is normally controlled by the magnitude of the interdimer coupling J'/k_B, i.e., increasing the value of J'/k_B widens the spacing between them. In such a scenario, the derivative of M, (dM/dH) vs H, should exhibit two peaks corresponding to H_{C1} and H_{C2} [16]. As presented in Fig. 3(b), our dM/dH vs H plot reveals only one peak at around 2.2 T, reflecting the fact that the compound is an isolated dimer system with negligible interdimer coupling [54]. C_p vs H measured at the lowest temperature of $T = 0.1$ K is shown in the inset of Fig. 4(b). C_p remains almost zero in low fields due to the singlet ground state. As the increasing field approaches H_{C1}, C_p starts increasing, shows a peak at around 2.2 T, and then decreases further to zero in higher fields [53]. Usually, in a system of coupled dimers with the spin gap, C_p vs H shows double peaks corresponding to H_{C1} and H_{C2} [15,55]. However, for an isolated dimer with negligible interdimer coupling, one may expect only one peak. In our case, we observed a single broad peak in $C_p(H)$ at $T = 0.1$ K that clearly indicates the proximity of our system to the isolated-dimer model where both H_{C1} and H_{C2} coincide when $T \to 0$.

D. Conclusion

Co-MOF features pseudospin-1/2 Co^{2+} dimers arranged in an orthogonal fashion, similar to the famous Shastry-Sutherland lattice. In zero-field, a quantum disordered ground state with the spin gap and no magnetic LRO is observed. The absence of magnetic LRO in applied fields down to 100 mK excludes BEC of triplons and underpins the absence of any significant interdimer coupling. We observed that the spin system deviates from the Heisenberg dimer limit. Indeed, the low-temperature properties are well described by an isolated spin-1/2 anisotropic *XXZ* dimer model ($J_{xy} \neq J_z$). No magnetization plateau is observed despite the presence of orthogonal dimers. However, this compound can serve as a model system to study magnetization plateaus if one can introduce a finite interdimer coupling by an appropriate choice of organic ligands.

ACKNOWLEDGMENTS

We would like to acknowledge SERB, India for financial support through Grant No. CRG/2022/000997. S.J.S. is supported by the Prime Minister's Research Fellowship (PMRF) scheme, Government of India. Computations for this work were done using resources of the Leipzig University Computing Center.

[1] S. Sachdev, Quantum phase transitions, Phys. World **12**, 33 (1999); M. Vojta, Quantum phase transitions, Rep. Prog. Phys. **66**, 2069 (2003).

[2] V. Zapf, M. Jaime, and C. D. Batista, Bose-Einstein condensation in quantum magnets, Rev. Mod. Phys. **86**, 563 (2014).

[3] T. M. Rice, To Condense or not to condense, Science **298**, 760 (2002).

[4] T. Giamarchi, C. Rüegg, and O. Tchernyshyov, Bose-Einstein condensation in magnetic insulators, Nat. Phys. **4**, 198 (2008).

[5] T. Nikuni, M. Oshikawa, A. Oosawa, and H. Tanaka, Bose-Einstein condensation of dilute magnons in $TlCuCl_3$, Phys. Rev. Lett. **84**, 5868 (2000).

[6] M. Jaime, V. F. Correa, N. Harrison, C. D. Batista, N. Kawashima, Y. Kazuma, G. A. Jorge, R. Stein, I. Heinmaa, S. A. Zvyagin, Y. Sasago, and K. Uchinokura, Magnetic-field-induced condensation of triplons in han purple pigment $BaCuSi_2O_6$, Phys. Rev. Lett. **93**, 087203 (2004).

[7] B. Thielemann, C. Rüegg, K. Kiefer, H. M. Rønnow, B. Normand, P. Bouillot, C. Kollath, E. Orignac, R. Citro, T. Giamarchi, A. M. Läuchli, D. Biner, K. Krämer, F. Wolff-Fabris, V. Zapf, M. Jaime, J. Stahn, N. B. Christensen, B. Grenier, D. F. McMorrow *et al.*, Field-controlled magnetic order in the quantum spin-ladder system $(Hpip)_2CuBr_4$, Phys. Rev. B **79**, 020408(R) (2009).

[8] V. O. Garlea, A. Zheludev, T. Masuda, H. Manaka, L.-P. Regnault, E. Ressouche, B. Grenier, J.-H. Chung, Y. Qiu, K. Habicht, K. Kiefer, and M. Boehm, Excitations from a Bose-Einstein condensate of magnons in coupled spin ladders, Phys. Rev. Lett. **98**, 167202 (2007).

[9] P. K. Mukharjee, K. M. Ranjith, B. Koo, J. Sichelschmidt, M. Baenitz, Y. Skourski, Y. Inagaki, Y. Furukawa, A. A. Tsirlin, and R. Nath, Bose-Einstein condensation of triplons close to the quantum critical point in the quasi-one-dimensional spin-$\frac{1}{2}$ antiferromagnet $NaVOPO_4$, Phys. Rev. B **100**, 144433 (2019).

[10] P. K. Mukharjee, K. M. Ranjith, M. Baenitz, Y. Skourski, A. A. Tsirlin, and R. Nath, Two types of alternating spin-$\frac{1}{2}$ chains and their field-induced transitions in $\varepsilon-LiVOPO_4$, Phys. Rev. B **101**, 224403 (2020).

[11] K. Kodama, M. Takigawa, M. Horvatić, C. Berthier, H. Kageyama, Y. Ueda, S. Miyahara, F. Becca, and F. Mila, Magnetic superstructure in the two-dimensional quantum antiferromagnet $SrCu_2(BO_3)_2$, Science **298**, 395 (2002).

[12] H. Kageyama, K. Yoshimura, R. Stern, N. V. Mushnikov, K. Onizuka, M. Kato, K. Kosuge, C. P. Slichter, T. Goto, and Y. Ueda, Exact dimer ground state and quantized magnetization plateaus in the two-dimensional spin system $SrCu_2(BO_3)_2$, Phys. Rev. Lett. **82**, 3168 (1999).

[13] N. Laflorencie and F. Mila, Theory of the field-induced BEC in the frustrated spin-$\frac{1}{2}$ dimer compound $BaCuSi_2O_6$, Phys. Rev. Lett. **102**, 060602 (2009).

[14] S. Suh, K. A. Al-Hassanieh, E. C. Samulon, I. R. Fisher, S. E. Brown, and C. D. Batista, Nonuniversal magnetization at the BEC critical field: Application to the spin dimer compound $Ba_3Mn_2O_8$, Phys. Rev. B **84**, 054413 (2011).

[15] R. S. Freitas, W. A. Alves, and A. Paduan-Filho, Magnetic-field-induced ordered phase in the chloro-bridged copper(ii) dimer system $[Cu_2(apyhist)_2Cl_2](ClO_4)_2$, Phys. Rev. B **95**, 184426 (2017).

[16] T. Lancaster, P. A. Goddard, S. J. Blundell, F. R. Foronda, S. Ghannadzadeh, J. S. Möller, P. J. Baker, F. L. Pratt, C. Baines, L. Huang, J. Wosnitza, R. D. McDonald, K. A. Modic, J. Singleton, C. V. Topping, T. A. W. Beale, F. Xiao, J. A. Schlueter, A. M. Barton, R. D. Cabrera *et al.*, Controlling magnetic order and quantum disorder in molecule-based magnets, Phys. Rev. Lett. **112**, 207201 (2014).

[17] V. S. Zapf, D. Zocco, B. R. Hansen, M. Jaime, N. Harrison, C. D. Batista, M. Kenzelmann, C. Niedermayer, A. Lacerda, and A. Paduan-Filho, Bose-Einstein condensation of $S = 1$ nickel spin degrees of freedom in $NiCl_2-4SC(NH_2)_2$, Phys. Rev. Lett. **96**, 077204 (2006).

[18] G. Hester, H. S. Nair, T. Reeder, D. R. Yahne, T. N. DeLazzer, L. Berges, D. Ziat, J. R. Neilson, A. A. Aczel, G. Sala, J. A. Quilliam, and K. A. Ross, Novel strongly spin-orbit coupled quantum dimer magnet: $Yb_2Si_2O_7$, Phys. Rev. Lett. **123**, 027201 (2019).

[19] K. Somesh, S. S. Islam, S. Mohanty, G. Simutis, Z. Guguchia, C. Wang, J. Sichelschmidt, M. Baenitz, and R. Nath, Absence of magnetic order and emergence of unconventional fluctuations in the $J_{\text{eff}} = \frac{1}{2}$ triangular-lattice antiferromagnet $YbBO_3$, Phys. Rev. B **107**, 064421 (2023).

[20] S. Mohanty, S. S. Islam, N. Winterhalter-Stocker, A. Jesche, G. Simutis, C. Wang, Z. Guguchia, J. Sichelschmidt, M. Baenitz, A. A. Tsirlin, P. Gegenwart, and R. Nath, Disordered ground state in the spin-orbit coupled $J_{\text{eff}} = \frac{1}{2}$ distorted honeycomb magnet $BiYbGeO_5$, Phys. Rev. B **108**, 134408 (2023).

[21] A. Abragam and M. H. L. Pryce, The theory of paramagnetic resonance in hydrated cobalt salts, Proc. R. Soc. A **206**, 173 (1951).

[22] G. Lin, J. Jeong, C. Kim, Y. Wang, Q. Huang, T. Masuda, S. Asai, S. Itoh, G. Günther, M. Russina, Z. Lu, J. Sheng, L. Wang, J. Wang, G. Wang, Q. Ren, C. Xi, W. Tong, L. Ling, Z. Liu *et al.*, Field-induced quantum spin disordered state in spin-1/2 honeycomb magnet $Na_2Co_2TeO_6$, Nat. Commun. **12**, 5559 (2021).

[23] X. Liu and H.-Y. Kee, Non-Kitaev versus Kitaev honeycomb cobaltates, Phys. Rev. B **107**, 054420 (2023).

[24] J. Sheng, L. Wang, A. Candini, W. Jiang, L. Huang, B. Xi, J. Zhao, H. Ge, N. Zhao, Y. Fu, J. Ren, J. Yang, P. Miao, X. Tong, D. Yu, S. Wang, Q. Liu, M. Kofu, R. Mole, G. Biasiol *et al.*, Two-dimensional quantum universality in the spin-1/2 triangular-lattice quantum antiferromagnet $Na_2BaCo(PO_4)_2$, Proc. Natl. Acad. Sci. USA **119**, e2211193119 (2022).

[25] Y. Gao, Y.-C. Fan, H. Li, F. Yang, X.-T. Zeng, X.-L. Sheng, R. Zhong, Y. Qi, Y. Wan, and W. Li, Spin supersolidity in nearly ideal easy-axis triangular quantum antiferromagnet $Na_2BaCo(PO_4)_2$, npj Quantum Mater. **7**, 89 (2022).

[26] M. O. Flynn, T. E. Baker, S. Jindal, and R. R. P. Singh, Two phases Inside the Bose condensation dome of $Yb_2Si_2O_7$, Phys. Rev. Lett. **126**, 067201 (2021).

[27] C. Feng, E. M. Stoudenmire, and A. Wietek, Bose-Einstein condensation in honeycomb dimer magnets and $Yb_2Si_2O_7$, Phys. Rev. B **107**, 205150 (2023).

[28] L.-C. Zhang, L. Zhang, G. Qin, Q.-R. Zheng, M. Hu, Q.-B. Yan, and G. Su, Two-dimensional magnetic metal–organic frameworks with the Shastry-Sutherland lattice, Chem. Sci. **10**, 10381 (2019).

[29] M. J. Coak, S. P. M. Curley, Z. Hawkhead, J. P. Tidey, D. Graf, S. J. Clark, P. Sengupta, Z. E. Manson, T. Lancaster, P. A. Goddard, and J. L. Manson, Asymmetric phase diagram and dimensional crossover in a system of spin-1/2 dimers under applied hydrostatic pressure, Phys. Rev. B **108**, 224431 (2023).

[30] Z.-W. Zhai, S.-H. Yang, M. Cao, L.-K. Li, C.-X. Du, and S.-Q. Zang, Rational design of three two-fold interpenetrated metal–organic frameworks: Luminescent Zn/Cd-Metal–organic

frameworks for detection of 2,4,6-trinitrophenol and nitrofurazone in the aqueous phase, Cryst. Growth Des. **18**, 7173 (2018).

[31] A. Nath, V. Kumar, A. Shukla, H. N. Ghosh, and S. Mandal, Influence of molecular separation on through-space intervalence transient charge transfer in metal–organic frameworks with cofacially arranged redox pairs, Angew. Chem. Intl. Ed. **62**, e202308034 (2023).

[32] A. Nath, G. M. Thomas, S. Hans, S. R. Vennapusa, and S. Mandal, Crystal packing-driven selective Hg(II) ion sensing using thiazolothiazole-based water-stable zinc metal–organic framework, Inorg. Chem. **61**, 2227 (2022).

[33] N. Qureshi, Mag2Pol: A program for the analysis of spherical neutron polarimetry, flipping ratio and integrated intensity data, J. Appl. Crystallogr. **52**, 175 (2019).

[34] B. Bauer, L. D. Carr, H. G. Evertz, A. Feiguin, J. Freire, S. Fuchs, L. Gamper, J. Gukelberger, E. Gull, S. Guertler, A. Hehn, R. Igarashi, S. V. Isakov, D. Koop, P. N. Ma, P. Mates, H. Matsuo, O. Parcollet, G. Pawłowski, J. D. Picon *et al.*, The ALPS project release 2.0: Open source software for strongly correlated systems, J. Stat. Mech. (2011) P05001.

[35] U. Arjun, K. M. Ranjith, B. Koo, J. Sichelschmidt, Y. Skourski, M. Baenitz, A. A. Tsirlin, and R. Nath, Singlet ground state in the alternating spin-$\frac{1}{2}$ chain compound $NaVOAsO_4$, Phys. Rev. B **99**, 014421 (2019).

[36] N. Ahmed, P. Khuntia, K. M. Ranjith, H. Rosner, M. Baenitz, A. A. Tsirlin, and R. Nath, Alternating spin chain compound $AgVOAsO_4$ probed by ^{75}As NMR, Phys. Rev. B **96**, 224423 (2017).

[37] A. Eichhöfer, Y. Lan, V. Mereacre, T. Bodenstein, and F. Weigend, Slow magnetic relaxation in trigonal-planar mononuclear Fe(II) and Co(II) Bis(trimethylsilyl)amido Complexes—A comparative study, Inorg. Chem. **53**, 1962 (2014).

[38] M. Iakovleva, T. Petersen, A. Alfonsov, Y. Skourski, H.-J. Grafe, E. Vavilova, R. Nath, L. Hozoi, and V. Kataev, Static magnetic and ESR spectroscopic properties of the dimer-chain antiferromagnet $BiCoPO_5$, Phys. Rev. Mater. **6**, 094413 (2022).

[39] M. E. Lines, Magnetic properties of $CoCl_2$ and $NiCl_2$, Phys. Rev. **131**, 546 (1963).

[40] T. Susuki, N. Kurita, T. Tanaka, H. Nojiri, A. Matsuo, K. Kindo, and H. Tanaka, Magnetization process and collective excitations in the S=1/2 triangular-lattice Heisenberg antiferromagnet $Ba_3CoSb_2O_9$, Phys. Rev. Lett. **110**, 267201 (2013).

[41] S. Lal, S. J. Sebastian, S. S. Islam, M. P. Saravanan, M. Uhlarz, Y. Skourski, and R. Nath, Double magnetic transitions and exotic field-induced phase in the triangular lattice antiferromagnets $Sr_3Co(Nb, Ta)_2O_9$, Phys. Rev. B **108**, 014429 (2023).

[42] N. Li, Q. Huang, X. Y. Yue, W. J. Chu, Q. Chen, E. S. Choi, X. Zhao, H. D. Zhou, and X. F. Sun, Possible itinerant excitations and quantum spin state transitions in the effective spin-1/2 triangular-lattice antiferromagnet $Na_2BaCo(PO_4)_2$, Nat. Commun. **11**, 4216 (2020).

[43] K. M. Ranjith, K. Brinda, U. Arjun, N. G. Hegde, and R. Nath, Double phase transition in the triangular antiferromagnet $Ba_3CoTa_2O_9$, J. Phys.: Condens. Matter **29**, 115804 (2017).

[44] U. Arjun, V. Kumar, P. K. Anjana, A. Thirumurugan, J. Sichelschmidt, A. V. Mahajan, and R. Nath, Singlet ground state in the spin-$\frac{1}{2}$ weakly coupled dimer compound $NH_4[(V_2O_3)_2(4,4'-bpy)_2(H_2PO_4)(PO_4)_2]\cdot 0.5H_2O$, Phys. Rev. B **95**, 174421 (2017).

[45] A. A. Tsirlin, R. Nath, J. Sichelschmidt, Y. Skourski, C. Geibel, and H. Rosner, Frustrated couplings between alternating spin-$\frac{1}{2}$ chains in $AgVOAsO_4$, Phys. Rev. B **83**, 144412 (2011).

[46] O. Nohadani, S. Wessel, and S. Haas, Quantum phase transitions in coupled dimer compounds, Phys. Rev. B **72**, 024440 (2005).

[47] H. Shiba, Y. Ueda, K. Okunishi, S. Kimura, and K. Kindo, Exchange interaction via crystal-field excited states and its importance in $CsCoCl_3$, J. Phys. Soc. Jpn. **72**, 2326 (2003).

[48] K. An, T. Sakakibara, R. Settai, Y. Onuki, M. Hiragi, M. Ichioka, and K. Machida, Sign reversal of field-angle resolved heat capacity oscillations in a heavy fermion superconductor $cecoin_5$ and $d_{x^2-y^2}$ pairing symmetry, Phys. Rev. Lett. **104**, 037002 (2010).

[49] R. Nath, M. Padmanabhan, S. Baby, A. Thirumurugan, D. Ehlers, M. Hemmida, H.-A. Krug von Nidda, and A. A. Tsirlin, Quasi-two-dimensional $S=\frac{1}{2}$ magnetism of $Cu[C_6H_2(COO)_4][C_2H_5NH_3]_2$, Phys. Rev. B **91**, 054409 (2015).

[50] C. Wellm, W. Roscher, J. Zeisner, A. Alfonsov, R. Zhong, R. J. Cava, A. Savoyant, R. Hayn, J. van den Brink, B. Büchner, O. Janson, and V. Kataev, Frustration enhanced by Kitaev exchange in a $j_{\text{eff}}=\frac{1}{2}$ triangular antiferromagnet, Phys. Rev. B **104**, L100420 (2021).

[51] E. Bartolome, P. J. Alonso, A. Arauzo, J. Luzón, J. Bartolome, C. Racles, and C. Turta, Magnetic properties of the seven-coordinated nanoporous framework material $Co(bpy)_{1.5}(NO_3)_2$ (bpy = 4,4′-bipyridine), Dalton Trans. **41**, 10382 (2012).

[52] H. Liu, J. Chaloupka, and G. Khaliullin, Kitaev spin liquid in $3d$ transition metal compounds, Phys. Rev. Lett. **125**, 047201 (2020).

[53] L. Pritchard Cairns, R. Day, S. Haley, N. Maksimovic, J. Rodriguez, H. Taghinejad, J. Singleton, and J. Analytis, Tracking the evolution from isolated dimers to many-body entanglement in $NaLu_xYb_{1-x}Se_2$, Phys. Rev. B **106**, 024404 (2022).

[54] A. A. Tsirlin, R. Nath, C. Geibel, and H. Rosner, Magnetic properties of $Ag_2VOP_2O_7$: An unexpected spin dimer system, Phys. Rev. B **77**, 104436 (2008).

[55] Y. Kohama, A. V. Sologubenko, N. R. Dilley, V. S. Zapf, M. Jaime, J. A. Mydosh, A. Paduan-Filho, K. A. Al-Hassanieh, P. Sengupta, S. Gangadharaiah, A. L. Chernyshev, and C. D. Batista, Thermal transport and strong mass renormalization in $NiCl_2{-}4SC(NH_2)_2$, Phys. Rev. Lett. **106**, 037203 (2011).